A THERMODYNAMIC ANALYSIS OF REFRIGERANTS: PERFORMANCE LIMITS OF THE VAPOR COMPRESSION CYCLE

Piotr A. Domanski*[(a)], J. Steven Brown[(b)], Jaehyeok Heo[(a)], Janusz Wojtusiak[(c)], and Mark O. McLinden [(d)]

[(a)]National Institute of Standards and Technology, Gaithersburg, MD 20899, United States

[(b)]The Catholic University of America, Washington, DC 20064, United States

[(c)]George Mason University, Fairfax, VA 22030, United States

[(d)]National Institute of Standards and Technology, Boulder, CO 20899, United States

ABSTRACT

This paper explores the thermodynamic performance limits of the vapor compression cycle. We have applied evolutionary algorithms to explore the performance of hypothetical refrigerants defined by the thermodynamic parameters used by the extended corresponding states model for fluid properties. We identified optimal values of these parameters required to reach the performance limits. The study confirmed the fundamental trade-off between the coefficient of performance (COP) and volumetric capacity, and indicated refrigerant critical temperature as the dominant parameter influencing the tradeoff. Thermodynamic performance limits depend on the operating conditions and the cycle design. These limits are represented by Pareto fronts developed for the objective functions COP and volumetric capacity. As expected, the performance of current refrigerants falls below the Pareto front limits. We demonstrate that for practical cycles the developed methodology and resulting Pareto fronts are more realistic benchmarks for the performance potentials of refrigerants than is COP alone, which is an efficiency only metric.

Keywords: coefficient of performance; evolutionary algorithm; refrigerant; vapor compression cycle;

*** Corresponding author.** Tel.: 1-301-975-5877; Fax: 1-301-975-8973.

E-mail address: piotr.domanski@nist.gov

This paper is an expanded version of the paper entitled "A Thermodynamic Analysis of Refrigerants. I. Thermodynamic Limits of the Vapor Compression Cycle" presented at the 4th IIR Conference on Thermophysical Properties and Transfer Processes of Refrigerants, Delft, The Netherlands, 2013

Draft version submitted to Int. Journal of Refrigeration
The final version is available at: http://dx.doi.org/10.1016/j.ijrefrig.2013.09.036

NOMENCLATURE

COP	coefficient of performance
C_p°	heat capacity in the limit of zero pressure (J mol^{-1} K^{-1})
ECS	extended corresponding states
EOS	equation of state
GWP	global warming potential
LL/SL-HX	liquid-line/suction-line heat exchanger
p	pressure (kPa)
Q_{vol}	volumetric heating or cooling capacity (kJ m^{-3})
T	temperature (˚C or K)
VCC	vapor compression cycle
α_1, α_2	shape factor fitting coefficients*
β_1, β_2	shape factor fitting coefficients*
ω	acentric factor
γ	C_p° temperature dependence parameter*

Subscripts:

cond	condenser inlet, dew point
evap	evaporator outlet, dew point

Superscript:

crit	critical point value

*used in the ECS model, see McLinden et al. (2012)

1. INTRODUCTION

The coefficient of performance (COP) and volumetric capacity (Q_{vol}) are two parameters, which stem from thermodynamic properties, which are used for characterizing the performance of a refrigerant in a vapor compression cycle (VCC). When it comes to presenting performance merits of different refrigerants, they are typically listed in the order of their COPs with their volumetric capacity given alongside. Often, a ratio of the COP_{VCC} to that of the Carnot cycle is used to benchmark the refrigerant performance against the ultimate thermodynamic limit of a fully reversible Carnot cycle. The COP_{VCC}/COP_{Carnot} index is not influenced by the volumetric capacity. This approach disregards the fundamental tradeoff between high Q_{vol} and high COP, which has been broadly noted and discussed in the literature (e.g., McLinden and Didion, 1987). However, there is no commonly accepted methodology to compare refrigerant performance based on both COP and Q_{vol}.

Theoretical VCCs come in several variations. Among single-stage cycles, the simple cycle consists of the compression process, heat rejection associated with high-pressure vapor desuperheating and condensation, adiabatic expansion in the throttling device, and heat absorption associated with liquid refrigerant evaporation. As compared to the Carnot cycle, the simple VCC suffers from thermodynamic irreversibilities associated with the adiabatic throttling process and desuperheating of the compressed vapor. The most common variation of the simple VCC − the cycle with a liquid-line/suction-line exchanger (LL/SL-HX) – improves COP for most refrigerants through reduction of throttling irreversibilities at the expense of some increase in compression work. Other variations of the simple VCC − cycles with the economizer, ejector, and expansion work recovery device – reduce throttling irreversibilities and the external work required for the compressions process. These “advanced” cycles improve COP for every refrigerant. The level of COP improvement depends on a refrigerant’s thermodynamic properties and varies from cycle to cycle (Domanski, 1995).

In this study we explore the thermodynamic performance limits for four different VCCs and identify optimal refrigerant thermodynamic parameters that lead to the best performance. Based on the obtained VCC performance limits represented by a Pareto front in terms of 1/COP and $1/Q_{vol}$, we propose a new approach for presenting the refrigerant cycle performance. This paper extends the work presented earlier by McLinden

et al. (2012). The findings on optimal refrigerant thermodynamic parameters are utilized in a search for low-GWP refrigerants reported in a companion paper (McLinden et al., 2013).

2. EXPLORATION OF THERMODYNAMIC SPACE

2.1 Exploration methodology

By the term "thermodynamic space" we denote a search domain containing refrigerant parameters (and their appropriate value ranges) which are chosen such that the full range of possible thermodynamic behaviors are encompassed. These parameters are those used by an equation of state (EOS) model for calculating the thermodynamic properties of a refrigerant. We explored the thermodynamic space with a VCC simulation model, which used thermodynamic refrigerant properties determined by the parameter values selected from this search domain. The goal of this exploration was to find an optimum combination of these parameters to maximize both COP and the Q_{vol}. COP is an indicator of the energy efficiency (operating cost) of the system. Q_{vol} is defined as the refrigeration capacity per unit volume of refrigerant vapor flowing into the compressor; it is a measure of equipment size (first cost). Since a fundamental tradeoff exists between COP and Q_{vol}, the employed exploration of thermodynamic space used a bi-objective optimization process. We may think of this exploration (optimization) process as an attempt to analytically "engineer" an optimal fluid by appropriate selection of parameter values from the thermodynamic space.

2.2 Representation of refrigerant properties

For the representation of refrigerant properties we employed the extended corresponding states (ECS) model of Huber and Ely (1994). The strength of the ECS approach is its ability to provide a representation of fluid properties with good accuracy given only a limited set of data or, for the present application, to provide thermodynamically consistent properties in terms of a limited number of parameters. This approach is not limited to fluids that are known, although corresponding states calculations are tied to real "reference fluids" and this ensures that thermodynamic consistency between properties is maintained. The NIST REFPROP database (Lemmon et al., 2010) implements the ECS model (among a number of thermodynamic models) and was used for the calculation of refrigerant properties in the cycle simulations. McLinden et al. (2012) present more detail on representation of refrigerant properties using the ECS approach.

The applied ECS model used nine refrigerant parameters; hence the thermodynamic space we explored was nine-dimensional. Table 1 lists the parameters that were varied in the optimization and their ranges. The critical temperature and pressure, T^{crit} and p^{crit}, are the upper limit of the two-phase "dome." The acentric factor ω is related to the slope of the vapor pressure curve with temperature. The ideal-gas heat capacity, C_p°, is the heat capacity of the vapor phase in the limit of zero pressure; C_p° is a function of temperature, and we focus here on its value at 300 K. T^{crit}, p^{crit}, ω, and C_p° are fundamental thermodynamic parameters of a fluid, and the others are fitting parameters for the model used; together they describe the thermodynamic behavior. Two reference fluids were used: propane and R-32. These two fluids are typical of non-polar and polar refrigerants, respectively, and both have very good equations of state that are valid over wide ranges of temperature and pressure—requirements for a reference fluid formulation.

Value ranges must be specified to constrain the optimization to physically reasonable bounds. The ranges given in Table 1 are based on the 105 pure fluids in REFPROP; these include all of the common refrigerants (both synthetic and natural) as well as additional simple organic and inorganic molecules that have boiling points in the range of current refrigerants. The critical temperature covers the range from near the condenser temperature in the cycles to be investigated here to a temperature near the critical temperature of water. All other parameters span the range of values observed for fluids in REFPROP, with only a few exceptions. Critical pressures lower than 2.0 MPa are observed only for hydrogen, helium, and complex molecules, which are not suitable for a vapor compression cycle at normal refrigeration temperatures. While water has a critical pressure of 22.064 MPa, the upper bound for the current optimization was set to 12 MPa, which is slightly above the next-highest p^{crit}, namely 11.333 MPa for ammonia. This greatly limits the search space for this parameter, a space that is not likely to contain any actual fluids. Negative values of the acentric factor ω are observed only for hydrogen and helium. Values of C_p°(300 K) larger than 300 $J \cdot mol^{-1} \cdot K^{-1}$ are observed for heavy hydrocarbons (greater than about C8), but again, these are not suitable for our application. The "granularity" is the smallest increment for a parameter deemed to have a significant impact on the solution.

2.3 Implementation of evolutionary algorithm

In general, the optimization process involves evaluating different candidate solutions from a given domain space and selecting the solution that is the "best one" for the given objectives. Our approach is to apply the principles of genetic optimization, whereby a set of candidate solutions (known as a "population" or "generation") are evaluated and the results are used to select "children", which are members for the next "population" to be assessed. The process is continued for a prescribed number of generations (Ashlock, 2006). In our case, candidate refrigerants are the "candidate solutions", and they are represented by a set of thermodynamic parameters. Through the optimization run, new members for the population are created by varying the values of these thermodynamic parameters with the objective to achieve the best COP and Q_{vol} values.

Multi-objective optimization − in most cases, including ours − does not provide a unique "best" solution satisfying every objective. In our case, the search algorithm will encounter, at first, fluids that have both better COP and Q_{vol} than those of the candidates it has evaluated thus far, but at some point it will no longer be possible to improve one objective without accepting lower values for the other. In multi-objective optimization, this fact is described by the term "Pareto optimality", and the collected tentative solutions are referred to as non-dominated (Goldberg, 1989). For our bi-objective problem, this set of non-dominated solutions forms the so-called Pareto front on the 1/COP-1/Q_{vol} plane. Hence, the Pareto front is a collection of fluids, which have the highest COP for a given Q_{vol}, and vice-versa, among all fluids evaluated, and it graphically represents the limit of performance that can actually be realized.

Optimization runs were executed by EOS-EVOL, a multi-objective evolutionary optimization tool developed for this work. EOS-EVOL worked in tandem with a cycle simulation model, which evaluated the refrigerant performance. For each member of the "population" (i.e., candidate refrigerant) EOS-EVOL generated sets of EOS parameters following its evolutionary scheme and provided these to the cycle model, which calculated the COP and Q_{vol} values. Upon completion of the optimization run, EOS-EVOL identified the solutions (*i.e.*, sets of fluid parameters) laying on the Pareto front for further "manual" analyses and interpretation.

EOS-EVOL can be classified as an evolutionary method, a type of population-based optimization method in which a set of candidate solutions (population) is used to generate new candidate solutions (children). EOS-EVOL combines random/semi-random operators traditionally used in evolutionary methods with guided machine-learning-based approaches (Wojtusiak and Michalski, 2006; Wojtusiak et al., 2012). The optimization run starts with a set of randomly generated candidate solutions, which constitute the first population. Then, new candidate solutions are created using (1) machine learning-based, (2) traditional evolutionary, and (3) random methods, as elaborated below. At this stage, the program also adjusts the precision of the parameters in the most promising search areas.

(1) Machine-learning-based creation of new candidate solutions is a two-step process. First, rule-learning software AQ21 (Wojtusiak et al. 2006) is applied to generate/learn hypotheses on why some candidate solutions perform better than others. The hypotheses, in the form of IF-THEN rules, capture areas of the parameter search space that are the most promising for further exploration. In other words, these areas are machine-learning-based generalizations of characteristics of candidate solutions near the Pareto front. Then, new candidate solutions are created by sampling these promising areas of the search space covered by rules.

(2) Traditional evolutionary operators include mutation and cross-over. Mutation randomly changes a candidate solution by modifying values of one or more parameters. Cross-over combines two "parent" candidate solutions by exchanging their parameters.

(3) Random generation produces new candidate solutions uniformly distributed in the search space. The main reason for using random generation is to prevent the method from getting stuck in local optima due to lack of diversity in the current population.

Newly created candidate solutions along with ones in the current population go through an evolutionary selection process to select the new population. This selection process combines principles of survival of the fittest in Darwinian evolution (here designs closest to the Pareto front are considered the fittest) with maintaining diversity in the population. The process of generating new candidate solutions and selecting new populations is repeated until stopping criteria are met. In the presented work EOS-EVOL was stopped after a

fixed number of generations, or when no further progress was made. The program returns a set of candidate solutions that constitute the Pareto front, or are close to the front.

We executed each optimization run using the following main EOS-EVOL control parameters: population size = 100; number of populations = 200; number of children/solutions generated for each population = 25; number of random candidate solutions in each population = 5. Accordingly, each optimization run examined $100 \times 200 = 20\,000$ candidate solutions. To obtain a sufficient number of non-dominated solutions to create a smooth Pareto front, we executed five optimization runs for each cycle option and application condition, which involved a total of 100 000 candidate fluids.

2.4 Cycle Analysis

A modified version of the cycle simulation model CYCLE_D, Version 5 (Brown et al., 2012) was used for the cycle analyses. The three operating conditions considered—cooling, refrigeration, and heating—were characterized by the temperatures in the condenser and evaporator. The evaporator superheat and condenser subcooling were assumed to be zero; the evaporator and the condenser were assumed to have no pressure drop; the refrigerant lines were assumed to have no pressure drop and no heat losses/gains to/from the ambient; and the compressor isentropic efficiency was assumed to be 100 %. For each application, four cycle configurations (see Figure 1) were studied: (a) the simple (baseline) cycle as described above, (b) the simple cycle with the inclusion of a liquid-line suction-line heat exchanger (LL/SL-HX effectiveness of 50 % and 100 % were considered), (c) an economizer cycle with two-stage compression, and (d) a cycle replacing the expansion device of the simple cycle with a work-recovery device (efficiencies of 50 % and 100 % were considered). These resulted in six cycle options, as listed in Table 2.

3. RESULTS

A total of 36 optimization cases (runs) resulted from the combination of three applications (cooling, heating, and refrigeration), six VCC options, and two reference fluids (R-32 and propane) for the ECS model. Approximately 1.2 million sets of thermodynamic parameters representing hypothetical fluids were simulated for each application. The goal of the optimization was to answer two fundamental questions:

- What are the thermodynamic limits for COP and Q_{vol} in a VCC?

- What thermodynamic parameters are most influential in bringing the refrigerant performance to those limits?

3.1 COP and Q_{vol} limits for the vapor compression cycle

The results were qualitatively similar for the three applications and two reference fluids. For presenting results of this study we selected the simulations obtained with R-32 used as the reference fluid; they were more robust than the propane-based simulations, i.e., they included extreme values of the COP and Q_{vol} ranges where propane-based simulations sometimes failed. The cooling case results were reported earlier by McLinden et al. (2012). The main results discussed here are for the refrigeration application.

Figure 2 presents the optimization results for four cycle options: the simple cycle, the cycle with a 100 % effective LL/SL-HX, the economizer cycle, and the cycle with 100 % efficient work recovery from the expansion process. For clarity, only those points defining the Pareto front are plotted. Following the convention in such optimizations, the inverse of COP and Q_{vol} are plotted, so that solutions satisfying reasonably well both objectives lie at the lower left corner. For comparison, the figure includes several selected refrigerants being developed or in current commercial use.

The figure demonstrates that the evolutionary optimizations yielded distinct Pareto fronts, suggesting that the starting populations, number of generations, and other parameters of the optimization process were appropriate. The Pareto front for the simple cycle is located farthest from each axis indicating the poorest performance among the various cycle options studied. Notice that the Pareto front for the cycle with 100 % expansion work recovery has a different shape than the other cycles and reaches the COP_{Carnot} limit for a wide range of Q_{vol}. This result is due to the 100 % efficient work recovery device used in our simulations; with the throttling irreversibilities eliminated, a fluid with an insignificant vapor superheat after compression will approach the COP of the Carnot cycle. The Pareto front for the cycle with 50 % work recovery (not shown in Figure 2) has a similar shape to the Pareto line for the economizer cycle.

Other than the cycle with a 100 % work recovery device, the Pareto fronts display asymptotic behavior for both COP and Q_{vol}; *i.e.*, they show the upper limit of COP or Q_{vol} that can be obtained if one is willing to accept a low value for the other parameter. The variation in COP has a total span of only 20 % compared to a

variation of Q_{vol} of up to two orders of magnitude. Different ranges (lengths) of the Pareto fronts on the charts result from convergence issues in property calculations for the hypothetical fluids when stressed to their thermodynamic limits. The cycle with a LL/SL-HX shows a lower Q_{vol} limit than the economizer cycle but a higher COP limit; however, one must bear in mind that this option assumed an idealized 100 % effective LL/SL-HX, which is not attainable in practice.

Figure 3 presents the COP of the Pareto front referenced to the COP_{Carnot} as a function of Q_{vol} for the simple cycle at the cooling and refrigeration operating conditions. The figure also includes COP/COP_{Carnot} values for selected refrigerants. Since the COP for the Pareto front is affected by Q_{vol} and the COP_{Carnot} is not, the COP/COP_{Carnot} line for the Pareto front departs from unity on the chart with increasing Q_{vol}. The COP deviation from the COP_{Carnot} is greater for the refrigeration application than the cooling application. This can be explained by the larger temperature lift ($T_{cond} - T_{evap}$) in the refrigeration application (50 K) than cooling (30 K), which increases irreversibilities due to vapor superheat during compression and throttling.

3.2 Optimal refrigerant EOS parameters

The optimization runs showed T^{crit}, p^{crit}, C_p° and ω to be the most influential EOS parameters. Figure 4 presents their distributions for the refrigerants forming the Pareto front for the refrigeration application for (a) the simple cycle, (b) the cycle with the LL/SL-HX with 50 % effectiveness, and (c) the cycle with the LL/SL-HX with 100 % effectiveness. Each set of vertically aligned symbols represents the EOS parameters for a single hypothetical refrigerant. The scale for the vertical axis normalizes the value of each parameter by its range given in Table 1; for example, normalized values of –1 and +1 represent T^{crit} values of 305 K and 605 K, respectively.

A common feature for all three cases is a strong positive dependence of COP on T^{crit}; it is the strongest trend shown on the charts. This is another representation of the COP versus Q_{vol} tradeoff. The cycles differ markedly in the location of symbols denoting C_p°; the optimal values for the simple cycle are at about 10 % above the bottom of its range; the optimal values increase to about 15 % for the cycle with the 50 % effective LL/SL-HX, and reach the upper limit ($C_p^\circ \approx 300$ J·mol^{-1}·K^{-1}) for the cycle with the 100 % effective LL/SL-HX. The optimal values for p^{crit} lay in the top 25 % and 10 % for the simple and LL/SL-HX cycles, respectively. The values of ω are consistently at the very bottom for all the cycles.

The other parameters had smaller effects on the COP and capacity; they are given in Figure 5. The values of α_2 and β_1 are consistently at the bottom and top, respectively, of their ranges. The optimal values of α_1 and β_2 show considerable scatter, indicating that there are no strong optimal values for these parameters. The remaining parameter, γ, is scattered for the simple cycle and is concentrated at the top of its range for the cycles with LL/SL-HX.

The optimal values of the key thermodynamic parameters (T^{crit}, p^{crit}, C_p° and ω) for the economizer cycle are very similar to those identified for the simple cycle. The reason is that the simple cycle and economizer cycle have the same "outline" on a thermodynamic diagram. The work recovery cycle differs in that the expansion process follows a path that is different than the constant enthalpy process of a throttling valve in the simple cycle; 100 % efficient work recovery is a constant entropy process, while the 50 % efficient work recovery case is intermediate between a constant-enthalpy process and a constant-entropy process. An interesting phenomenon is the dependence of the optimum C_p° value on the efficiency of the work recovery cycle; the higher the efficiency of work recovery, the higher is the optimum value of C_p°, as it was also observed for the LL/SL-HX cycle where the optimal value of C_p° was affected by the effectiveness of the LL/SL-HX.

Similar to the COP charts shown in Figure 4, a Q_{vol} chart can be constructed as presented by McLinden et al (2012). Such a chart presents the same data sets as those in the COP chart except that they are sorted and displayed in order of increasing volumetric capacity. Thus to some degree, the Q_{vol} chart is a mirror image of the COP chart, which is consistent with the COP versus Q_{vol} tradeoff demonstrated by the Pareto front.

The implications of the thermodynamic analysis for refrigerant selection are as follows: Select a refrigerant with a critical temperature based on the economic tradeoff between first costs and operating costs that is appropriate for the application. Select a refrigerant with as high a value of critical pressure and as low a value of acentric factor as possible given the other constraints. The C_p° should be low for the simple vapor compression cycle or higher for a cycle with liquid line/suction line heat exchange. Or, conversely, this last point can be interpreted as: implement a LL/SL-HX (or other cycle modifications) as appropriate to match the thermodynamic characteristics of the refrigerant.

3.3 Performance of current refrigerants

The currently used refrigerants are located well away from the Pareto front for every cycle configuration, except for 100 % work recovery. The relative location of these refrigerants on the different charts indicates that different cycle modifications will have different effects depending on the thermodynamic properties of the individual refrigerants. The currently used refrigerants are most widely scattered on the simple cycle chart (Figure 2a), and are most tightly grouped for the cycle with work recovery (Figure 2d). The work recovery device improved COP for every fluid; however, it provided a larger COP improvement for poorer performers than for better- performing fluids. The economizer cycle also improved COP for every refrigerant but to a smaller degree than the work recovery cycle. The cycle with the LL/SL-HX provided a mixed influence depending on the molar heat capacity of the refrigerant (Domanski et al., 1994). For example, compared to the simple cycle, the COPs for propane and R-125 (large heat capacities) improved in the cycle with the LL/SL-HX, while the COPs for ammonia (NH_3) and R-32 (small heat capacities) decreased. It is interesting to note that the performance of R-1234yf (a HFO of considerable industrial interest) is substantially improved by the addition of a LL/SL-HX.

Figure 3 shows how COPs of the current refrigerants deviate from the Pareto front COPs. It is easy to see how the concept of the Pareto front as a representation of the performance limit on the 1/COP-1/Q_{vol} plane can be used to obtain a more insightful comparison of the performances of different refrigerants than the commonly used comparison based on COP alone. Specifically, a ratio of the evaluated refrigerant COP to the COP of the "optimal" refrigerant represented on the Pareto front and having the same Q_{vol} as the evaluated refrigerant would introduce to refrigerant benchmarking the fundamental tradeoff between COP and Q_{vol}, which is lacking when the absolute COP value is used or referenced to the COP_{Carnot}.

4. CONCLUSIONS

We have employed evolutionary optimization techniques, a theoretical cycle model, and the ECS model for representation of refrigerant thermodynamic properties to outline the upper performance limits of a vapor compression cycle (VCC) in terms of COP and Q_{vol} for four cycle variations. We identified optimal values of refrigerant thermodynamic parameters required to reach these performance limits. The identified "optimal fluids" form a Pareto front on coordinates of 1/COP versus 1/Q_{vol} representing the best performance that is

allowed by thermodynamics. The study confirmed the fundamental tradeoff between the COP and Q_{vol}, and indicated T^{crit} as the most dominant parameter influencing it. As expected, performance of current refrigerants falls below the Pareto front.

The obtained information can be helpful in preliminary screening of refrigerant candidates, which should be followed by rigorous modeling once a complete set of thermodynamic data is available. The VCC performance limits, as represented by the Pareto front, can be used to express the performance of a refrigerant by relating its COP to the COP of the "thermodynamically optimal" refrigerant having the same volumetric capacity as the evaluated refrigerant. This approach provides a more equitable benchmarking when refrigerants of different volumetric capacities are evaluated and compared.

ACKNOWLEDGEMENTS

This work was supported by the U.S. Department of Energy, Office of Energy Efficiency and Renewable Energy under contract no. DE-EE002057 with A. Bouza and B. Habibzadeh serving as Project Managers. We also thank our collaborators J. Filliben and A. Pintar of the NIST Statistical Engineering Division.

REFERENCES

Ashlock, D., 2006. Evolutionary Computation for Modeling and Optimization. Springer: New York, NY.

Brown, J.S., Domanski, P.A., and Lemmon, E.W., 2012. NIST Standard Reference Database 49, CYCLED: NIST Vapor Compression Cycle Design Program, version 5.0. National Institute of Standards and Technology, Gaithersburg, MD.

Domanski, P. A., Didion, D. A., Doyle, J. P., 1994. Evaluation of suction-line/liquid-line heat exchange in the refrigeration cycle. Int. J. Refrigeration 17 (7), 487-493.

Domanski, P.A., 1995. Minimizing Throttling Losses in the Refrigeration Cycle. Proceedings of the Int. Congress of Refrigeration, The Hague, The Netherlands, August 21-25, 1995, Int. Inst. Refrig., Paris, France, 766-773.

Goldberg, D. E. 1989. Genetic Algorithms in Search, Optimization, and Machine Learning. Addison Wesley Longman, Inc.: Reading, MA.

Huber, M.L. and Ely, J.F., 1994. A predictive extended corresponding states model for pure and mixed refrigerants including an equation of state for R-134a. Int. J. Refrigeration. 17, 18-31.

Lemmon, E. W., Huber, M. L., McLinden, M. O. 2013. NIST Standard Reference Database 23, NIST Reference Fluid Thermodynamic and Transport Properties - REFPROP, version 9.1. Standard Reference Data Program, National Institute of Standards and Technology, Gaithersburg, MD.

McLinden, M.O., Didion, A.D., 1987. Quest for alternatives, ASHRAE Journal. 29(12), 32-42.

McLinden, M.O., Domanski, P.A., Kazakow, A., Heo, J., Brown, J.S., 2012. Possibilities, Limits, and Tradeoffs for Refrigerants in the Vapor Compression Cycle, ASHRAE/NIST Refrigerants Conference, October 29-30, 2012, Gaithersburg, MD.

McLinden, M.O., Kazakow, A., Brown, J.S., Domanski, P.A., 2013. A Thermodynamic Analysis of Refrigerants: Possibilities and Tradeoffs for Low-GWP Refrigerants. Int. J. Refrigeration (in press).

Wojtusiak, J.; Michalski, R. S., 2006. The LEM3 Implementation of Learnable Evolution Model and Its Testing on Complex Function Optimization Problems. Genetic and Evolutionary Computation Conference, GECCO, Seattle, WA.

Wojtusiak, J., Warden, T. and Herzog, O., 2012. The learnable evolution model in agent-based delivery optimization. Memetic Computing, 4(3), 165-181

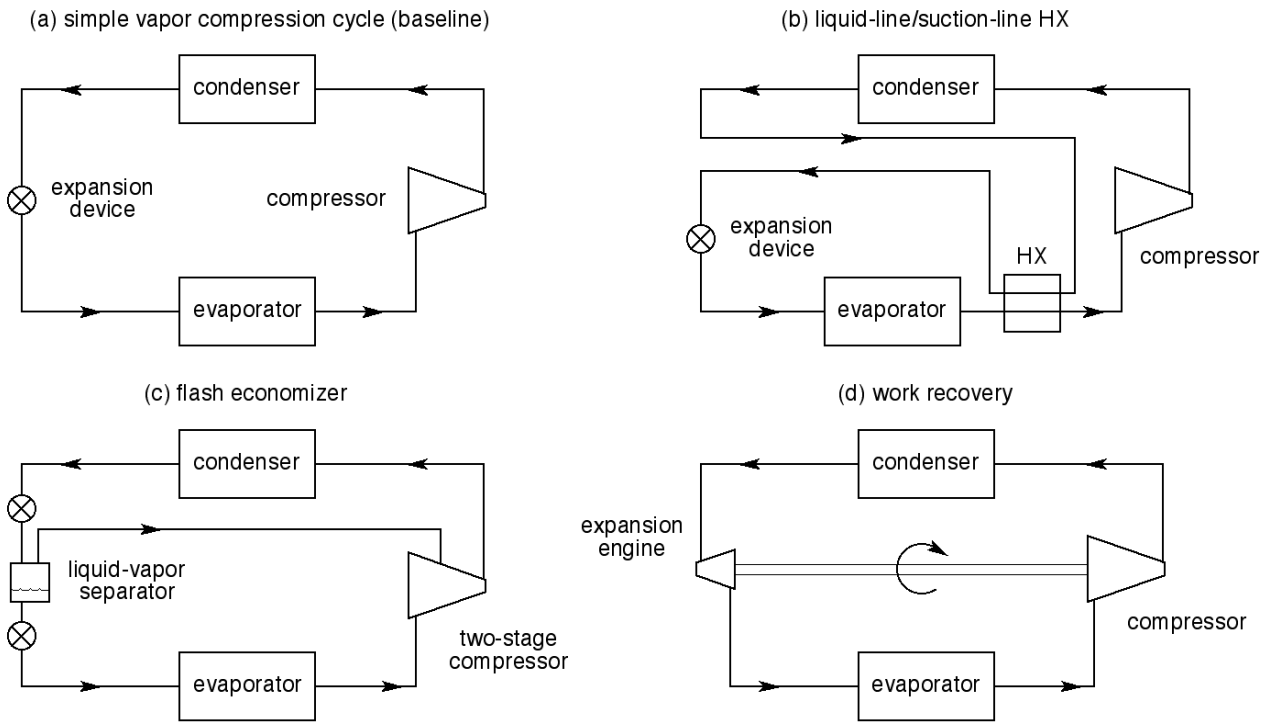

Figure 1. Vapor compression cycles studied: (a) simple (baseline) vapor compression cycle; (b) cycle with LL/SL-HX (effectivenesses of 50 % or 100 %); (c) economizer cycle with two-stage compression; and (d) cycle with work recovery from expansion device (efficiency of 50 % or 100 %).

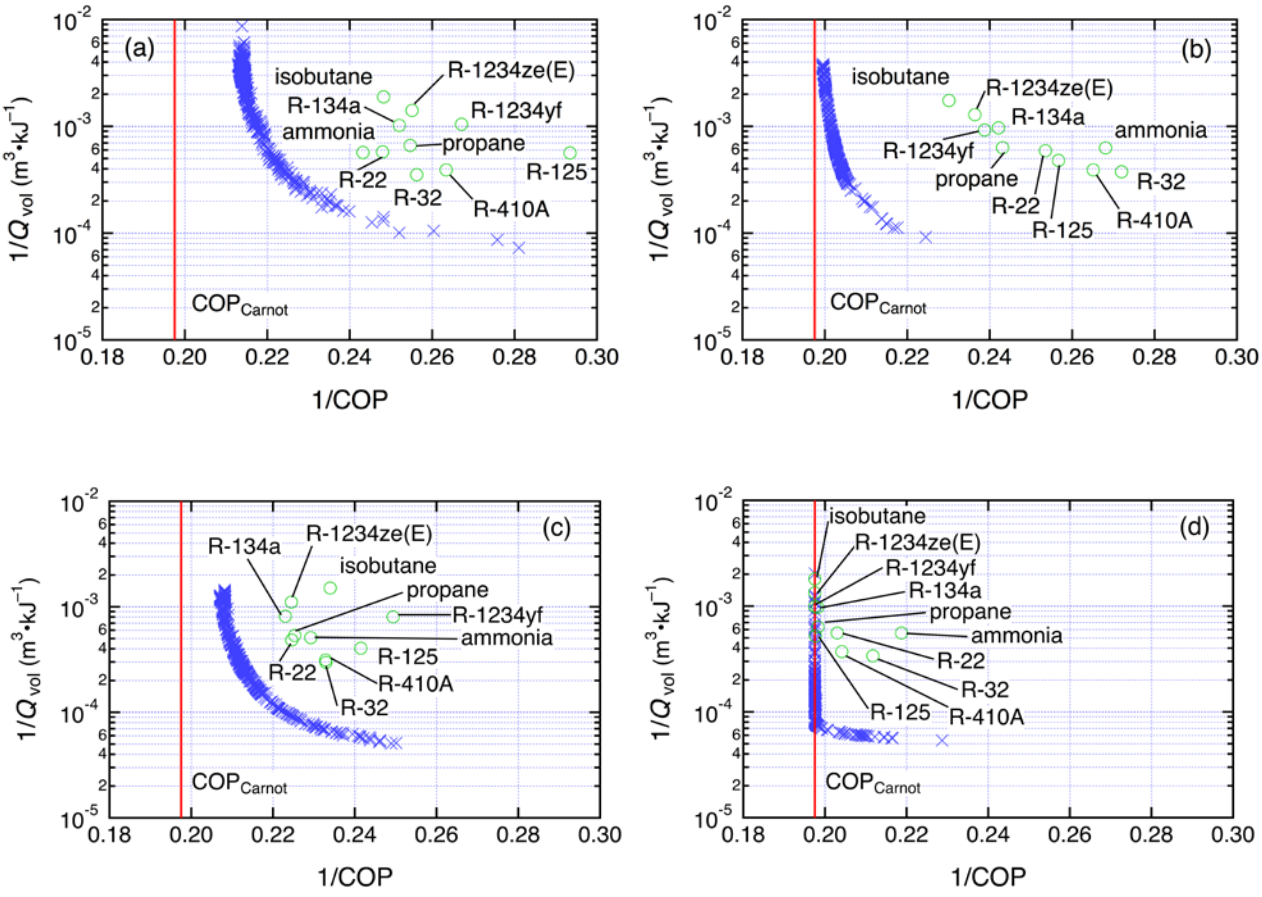

Figure 2. Pareto front (×), and selected refrigerants (○) for a refrigeration application and different cycle options: (a) simple VCC; (b) cycle with 100 % effective LL/SL-HX; (c) economizer cycle; and (d) cycle with 100 % efficient work recovery.

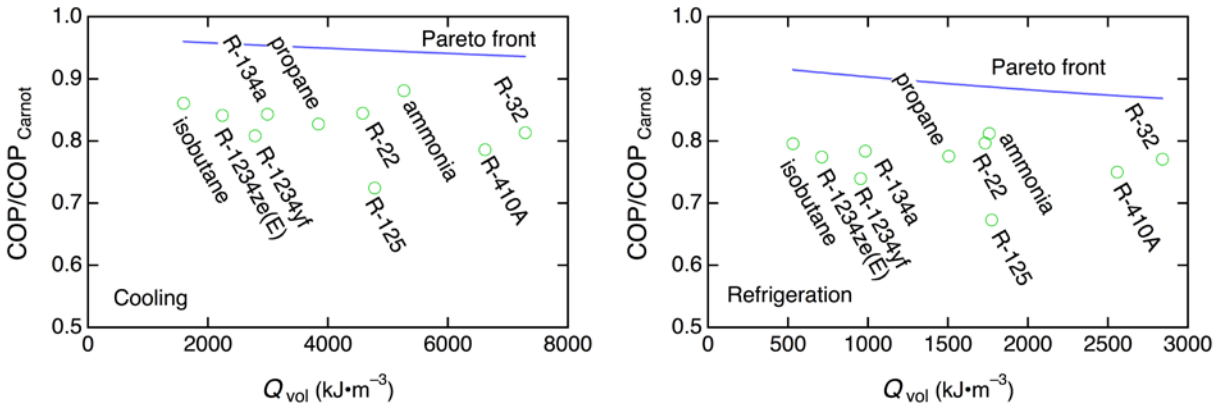

Figure 3. COP of Pareto front and selected refrigerants referenced to COP_{Carnot} for simple cycle for cooling and refrigeration applications.

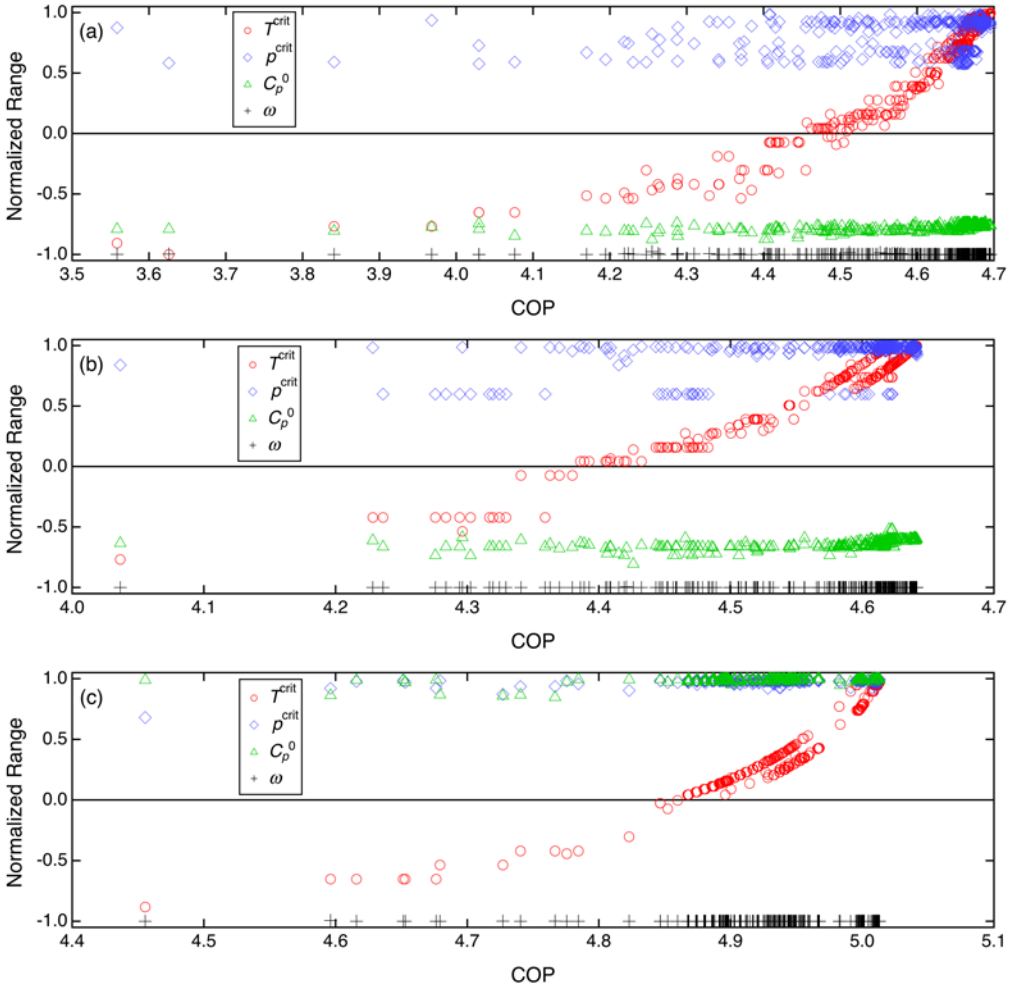

Figure 4. Refrigerant parameters (T^{crit}, p^{crit}, C_p° and ω) normalized by the ranges defined in Table 1 and ordered by COP for fluids on the Pareto front for the different cycle options: (a) simple VCC; (b) cycle with 50 % effective LL/SL-HX; (c) cycle with 100 % effective LL/SL-HX.

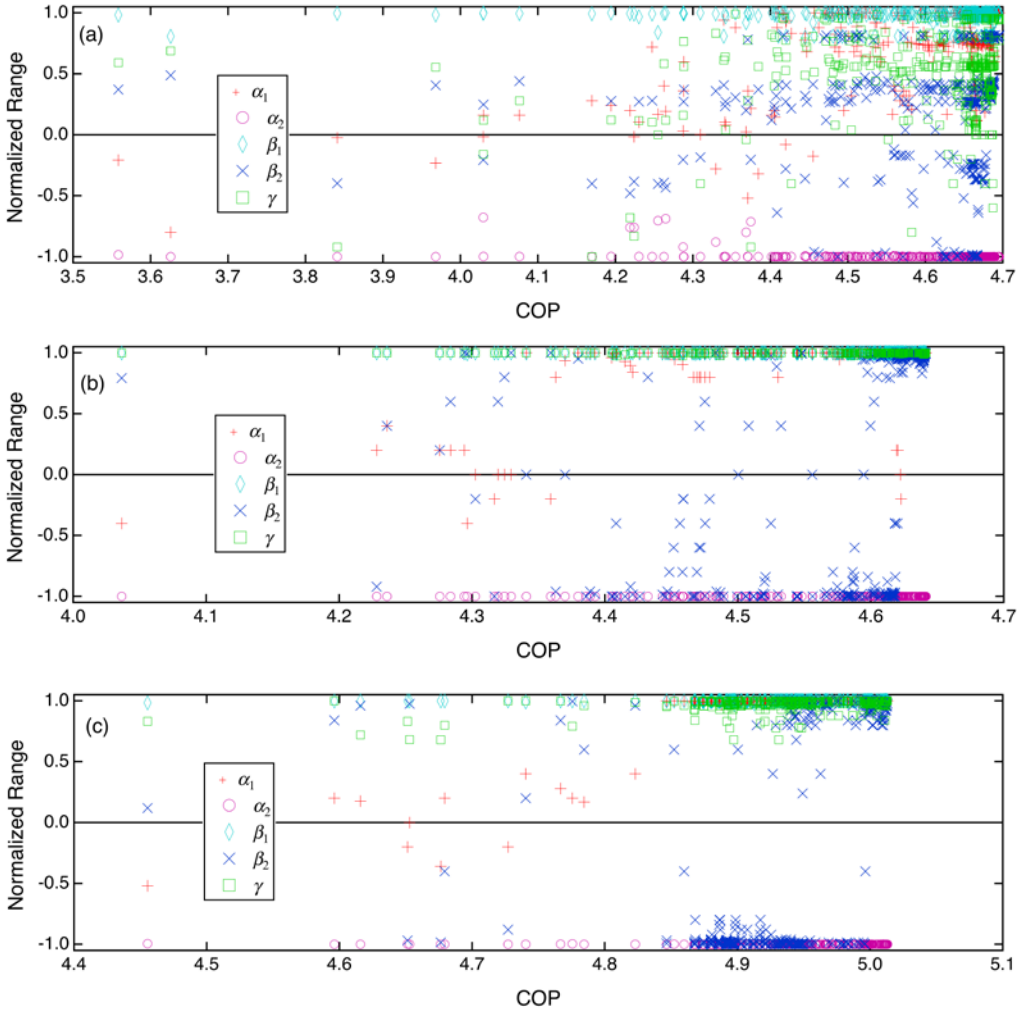

Figure 5. Refrigerant parameters (α_1, α_2, β_1, β_2, and γ) normalized by the ranges defined in Table 1 and ordered by COP for fluids on the Pareto front for the different cycle options: (a) simple VCC; (b) cycle with 50 % effective LL/SL-HX; (c) cycle with 100 % effective LL/SL-HX.

Figure caption

Figure 1. Vapor compression cycles studied: (a) simple (baseline) vapor compression cycle; (b) cycle with LL/SL-HX (effectivenesses of 50 % or 100 %); (c) economizer cycle with two-stage compression; and (d) cycle with work recovery from expansion device (efficiency of 50 % or 100 %).

Figure 2. Pareto front (×), and selected refrigerants (○) for a refrigeration application and different cycle options: (a) simple VCC; (b) cycle with 100 % effective LL/SL-HX; (c) economizer cycle; and (d) cycle with 100 % efficient work recovery.

Figure 3. COP of Pareto front and selected refrigerants referenced to COP_{Carnot} for simple cycle for cooling and refrigeration applications.

Figure 4. Refrigerant parameters (T^{crit}, p^{crit}, C_p° and ω) normalized by the ranges defined in Table 1 and ordered by COP for fluids on the Pareto front for the different cycle options: (a) simple VCC; (b) cycle with 50 % effective LL/SL-HX; (c) cycle with 100 % effective LL/SL-HX.

Figure 5. Refrigerant parameters (α_1, α_2, β_1, β_2, and γ) normalized by the ranges defined in Table 1 and ordered by COP for fluids on the Pareto front for the different cycle options: (a) simple VCC; (b) cycle with 50 % effective LL/SL-HX; (c) cycle with 100 % effective LL/SL-HX.

Table 1. ECS Fluid Parameters Varied in the Optimization Runs, and Their Ranges and Granularity

Parameter	Units	Range	Granularity
T^{crit}	K	305 to 650	0.5
p^{crit}	MPa	2.0 to 12.0	0.05
ω	–	0.0 to +0.6	0.005
α_1	–	–0.3 to +0.3	0.01
α_2	–	–0.8 to 0.0	0.1
β_1	–	–1.0 to +1.0	0.01
β_2	–	–0.8 to +0.8	0.1
C_p°(300 K)	$J \cdot mol^{-1} \cdot K^{-1}$	20.8 to 300	0.2
γ	K^{-1}	0.0 to 0.0025	0.0001

Table 2. Cycle Simulation Cases

Application	T_{evap} **(°C)**	T_{cond} **(°C)**	**Cycle option**	**Upgrade over baseline cycle**
Cooling	10	40	1	None
			2	LL/SL-HX; 50 % effectiveness
			3	LL/SL-HX; 100 % effectiveness
			4	Economizer; optimized intermediate pressure
			5	Work recovery device; 50 % efficiency
			6	Work recovery device; 100 % efficiency
Commercial Refrigeration	–20	30	As Above	As above
Heating	–10	30	As Above	As above